

Synthetic developmental regulator MciZ targets FtsZ across *Bacillus* species and inhibits bacterial division

Lidia Araújo-Bazán,^{1*} Sonia Huecas,¹ Javier Valle,²
David Andreu² and José M. Andreu^{1*} 

¹Centro de Investigaciones Biológicas, CSIC, Madrid, Spain.

²Department of Experimental and Health Sciences, Universitat Pompeu Fabra, Barcelona, Spain.

Summary

Cell division in most bacteria is directed by FtsZ, a conserved tubulin-like GTPase that assembles forming the cytokinetic Z-ring and constitutes a target for the discovery of new antibiotics. The developmental regulator MciZ, a 40-amino acid peptide endogenously produced during *Bacillus subtilis* sporulation, halts cytokinesis in the mother cell by inhibiting FtsZ. The crystal structure of a FtsZ:MciZ complex revealed that bound MciZ extends the C-terminal β -sheet of FtsZ blocking its assembly interface. Here we demonstrate that exogenously added MciZ specifically inhibits *B. subtilis* cell division, sporulation and germination, and provide insight into MciZ molecular recognition by FtsZ from different bacteria. MciZ and FtsZ form a complex with sub-micromolar affinity, analyzed by analytical ultracentrifugation, laser biolayer interferometry and isothermal titration calorimetry. Synthetic MciZ analogs, carrying single amino acid substitutions impairing MciZ β -strand formation or hydrogen bonding to FtsZ, show a gradual reduction in affinity that resembles their impaired activity in bacteria. Gene sequences encoding MciZ spread across genus *Bacillus* and synthetic MciZ slows down cell division in *Bacillus* species, including pathogenic *Bacillus cereus* and *Bacillus anthracis*. Moreover, *B. subtilis* MciZ is recognized by the homologous FtsZ from *Staphylococcus aureus* and inhibits division when it is expressed into *S. aureus* cells.

Introduction

Bacterial cell division is carried out by the concerted action of a macromolecular complex called the divisome (den Blaauwen *et al.*, 2017) and the cell wall synthesizing enzymes at the cytokinesis site (Egan *et al.*, 2017). Divisomal assembly is initiated in most bacteria by the formation of a ring-like scaffold of the cytoskeletal protein FtsZ at the nascent division site (Bi and Lutkenhaus, 1991). The Z-ring is attached to the inner side of the plasma membrane by membrane tethering proteins and recruits the rest of the division machinery (Haeusser and Margolin, 2016; Xiao and Goley, 2016; Du and Lutkenhaus, 2017). The Z-ring precisely localizes to the mid cell by means of different regulatory factors that either induce FtsZ assembly at the division site or prevent FtsZ assembly at the poles or over unsegregated chromosomes (den Blaauwen *et al.*, 2017). In addition, metabolic sensors inhibit FtsZ assembly and control cytokinesis in response to the nutritional state of the cell (Weart *et al.*, 2007; Monahan and Harry, 2016). The Z-ring has a fast subunit turnover (Anderson *et al.*, 2004) and is composed of discrete FtsZ clusters that circumferentially treadmill guiding septal cell wall synthesis (Bisson-Filho *et al.*, 2017; Yang *et al.*, 2017; Monteiro *et al.*, 2018), leading to the scission of daughter cells. FtsZ is a tubulin-like GTPase whose subunits assemble head-to-tail forming polar filaments (Nogales *et al.*, 1998; Matsui *et al.*, 2012) that laterally associate into bundles through the disordered C-terminal tails (Buske *et al.*, 2015; Huecas *et al.*, 2017; Sundararajan *et al.*, 2018). GTP hydrolysis at the interface between monomers in filaments and a polymerization-driven structural switch enable FtsZ filament treadmill dynamics (Artola *et al.*, 2017; Wagstaff *et al.*, 2017).

Due to its essential function in most bacteria, FtsZ is an attractive target (Lock and Harry, 2008), still clinically unexplored, for discovering new antibiotics that are urgently needed to counter the spread of resistant pathogens. FtsZ inhibition blocks cell division, inducing the formation of larger undivided cells that subsequently die. Many experimental small molecule FtsZ inhibitors have been reported (Schaffner-Barbero *et al.*, 2012; den Blaauwen *et al.*, 2014), including GTP-replacing

Accepted 2 January, 2019. *For correspondence. E-mail lidiaarba@gmail.com (Lidia Araújo-Bazán); j.m.andreu@cib.csic.es (José M. Andreu); Tel. (+34) 918373112; Fax (+34) 915360432.

inhibitors (Ruiz-Avila *et al.*, 2013; Artola *et al.*, 2015) and allosteric modulators of the structural assembly switch (Elsen *et al.*, 2012; Artola *et al.*, 2017). The difluorobenzamide derivative PC190723 (Haydon *et al.*, 2008) and several of its analogs are currently the best characterized FtsZ-targeting antibacterial inhibitors, including biochemical, structural, cellular and resistance mechanisms (Andreu *et al.*, 2010; Matsui *et al.*, 2012; Tan *et al.*, 2012; Stokes *et al.*, 2013; Adams *et al.*, 2016; Kaul *et al.*, 2016; Fujita *et al.*, 2017).

Starvation or harsh conditions induce *B. subtilis* cells to exit vegetative growth and binary fission and enter asymmetric sporulation, a form of reproduction that ensures storage and dissemination of the bacterial germline, until conditions permit spore germination and resuming growth. Increasing levels of the phosphorylated transcription regulator Spo0A promote the Z-ring localization switch from mid cell to the poles (Levin and Losick, 1996). Distinct programs of gene expression are initiated in the two cell types directed by sporulation-specific RNA polymerase σ factors, σ^F becoming active in the prespore and σ^E in the mother cell (Errington, 2003; Piggot and Hilbert, 2004). MciZ is a 40-amino acid developmental regulator that was discovered in a two-hybrid screen for FtsZ binding partners. MciZ is expressed during sporulation under the control of transcription factor σ^E , preventing Z-ring formation in the mother cell (Handler *et al.*, 2008). The crystal structure of a FtsZ:MciZ complex, formed by coexpressing His-tagged MciZ and a truncated version of *B. subtilis* FtsZ(12-315) including only the structured core of the protein, has revealed that MciZ binds at the C-terminal polymerization interface of FtsZ, structurally equivalent to the minus end of tubulin, inhibiting FtsZ assembly by steric hindrance and shortening protofilaments (Bisson-Filho *et al.*, 2015). The cell division inhibitor SulA, which is expressed as part of the SOS system and stalls cell division in response to DNA damage, also binds the C-terminal polymerization interface (Cordell *et al.*, 2003).

We determined the cytological profile on *B. subtilis* cells of inhibitors targeting FtsZ on different binding sites, distinguishing them from antibiotics with other mechanisms of action, which should facilitate phenotypic screening. In addition to small molecules, a MciZ synthetic peptide was observed to inhibit *B. subtilis* cell division (Araujo-Bazan *et al.*, 2016). However, it was not known whether exogenous MciZ really targets intracellular FtsZ; and the possibility that MciZ could arrest cell division in other bacterial species had not been examined. Here, we analyze the molecular recognition by different FtsZs of MciZ and peptide analogs with point changes, demonstrating FtsZ targeting in *B. subtilis* cells. In addition to cell division, excess MciZ inhibits sporulation and germination. MciZ homologs are encoded by other *Bacillus* species, and sensitivity to synthetic MciZ reaches pathogenic *B. cereus/anthracis*. We

show that MciZ is also recognized by FtsZ from *S. aureus* and that intracellular expression of MciZ inhibits *S. aureus* cell division.

Results and discussion

Exogenous MciZ specifically inhibits Bacillus subtilis cell division

To quantify the action of synthetic MciZ on cell division, we exposed cells to different concentrations of MciZ and determined cell length at different times (Fig. 1). The minimal concentration that inhibits *B. subtilis* cell division is 1 μ M MciZ (Fig. 1A and B), according to our criterion to identify relevant inhibitors by induction of a strong filamentous phenotype (\geq threefold increase in mean cell length, 3.1-fold here; Araujo-Bazan *et al.*, 2016). As expected for cell division inhibition (Arjes *et al.*, 2014), MciZ does not affect initial growth at this concentration: the mass doubling period (MDP) is the same as for control (Table S1). Higher concentrations of MciZ, 2.5 and 5 μ M, induce a 7-fold and 12-fold increase in cell length while the increment in MDP is only 1.07-fold and 1.44-fold respectively. The minimal division inhibitory concentration is 10-fold smaller than the minimum inhibitory concentration of growth (MIC₉₀), 10 μ M MciZ, supporting specific divisomal inhibition rather than general toxicity effects. We compared the time course of MciZ action with PC190723 a reference small molecule FtsZ inhibitor (Haydon *et al.*, 2008) (Fig. 1C). Both inhibitors had parallel filamenting effects: a relevant increase in cell length was observed following 80 min treatment with MciZ or PC190723. However, each inhibitor works by a different mechanism: MciZ blocks FtsZ polymer growth (Bisson-Filho *et al.*, 2015), whereas PC190723 binding stabilizes FtsZ polymers (Andreu *et al.*, 2010; Elsen *et al.*, 2012). MciZ increases the velocity of the directional treadmilling movement of NeonGreen-FtsZ around the division ring, whereas PC190723 halts FtsZ movement (Bisson-Filho *et al.*, 2017). Thus, the available evidence indicated that exogenous MciZ is a specific inhibitor of *B. subtilis* cell division, which led us to an in-depth study of the molecular mechanisms of MciZ action on bacterial cells.

Structure-based single amino acid changes in synthetic MciZ support FtsZ targeting in B. subtilis cells

The crystal structure of the core FtsZ:MciZ complex showed that MciZ binds to the C-terminal subdomain of FtsZ, sterically interfering at the association interface with a next monomer to form FtsZ filaments (Bisson-Filho *et al.*, 2015). Bound MciZ folds into a α -helix (H1) preceded by a β -hairpin, formed by strands β 1 and β 2 that are disordered in free MciZ, and followed by a loop and

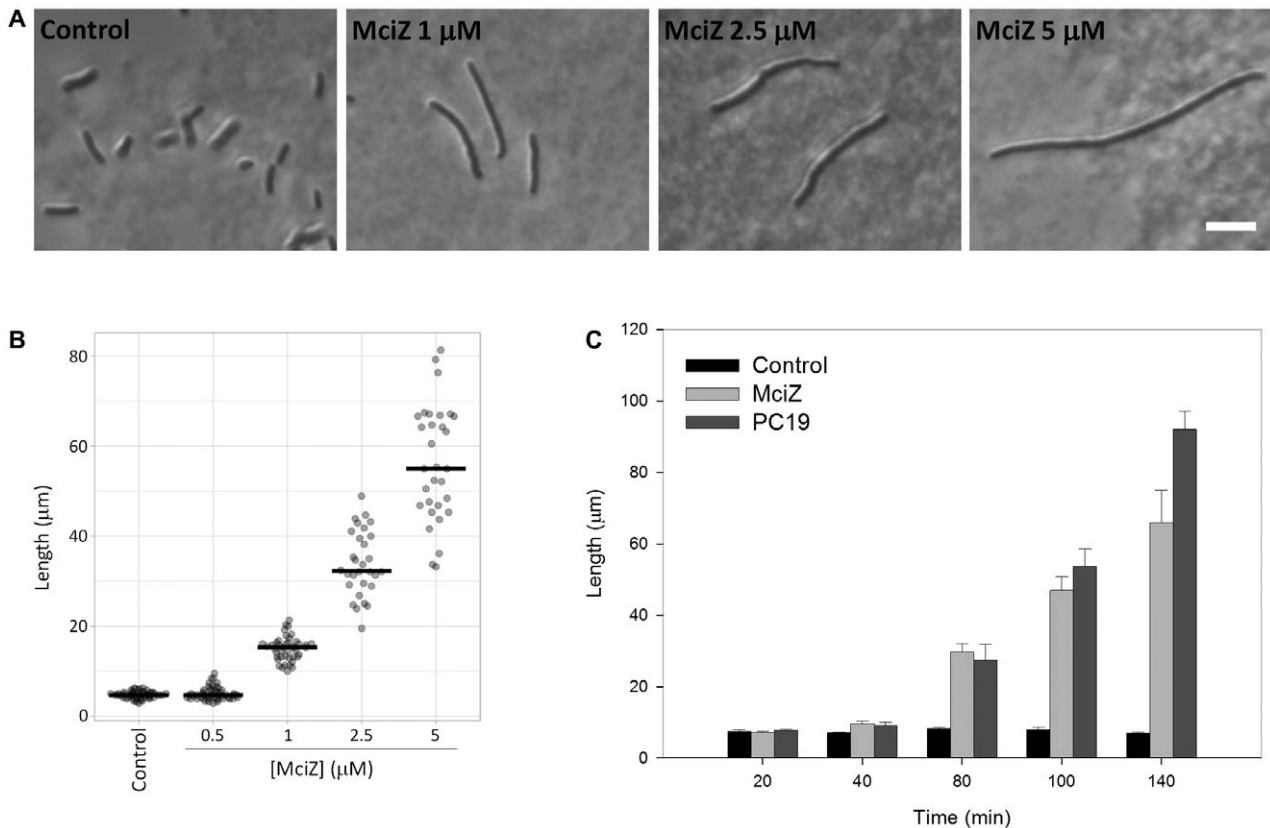


Fig. 1. Synthetic peptide MciZ inhibits *B. subtilis* cell division.

A. Representative examples of undivided *B. subtilis* 168 cells incubated with different MciZ concentrations during 1.5 h (phase contrast; scale bar: 10 μm).

B. Cell length measurements. Raw data plots with mean values ($n \geq 30$).

C. Time course of the effect of MciZ (5 μM) on cell length compared with the small molecule cell division inhibitor PC190723 (5 μM). The histogram shows the average and standard error from three independent experiments with $n \geq 30$.

a helical turn. Backbone hydrogen bonds between FtsZ strand $\beta 9$ and MciZ strand $\beta 2$ generate an extended β -sheet. There are hydrophobic interactions between helices H1 of MciZ and H10 of FtsZ, and between the $\beta 2$ /H1 loop of MciZ and the H10/ $\beta 9$ loop of FtsZ; a salt bridge between Arg20 of MciZ (H1) and Asp280 of FtsZ (H10) further stabilizes the complex (Fig. 2A and B).

We decided to challenge the MciZ:FtsZ recognition with synthetic point mutations in MciZ designed to disable these interactions (Fig. 2C), testing the effects of the modified synthetic peptides on living *B. subtilis* cells (Figs. 2D, S1, Tables S1 and S2). We first eliminated the Arg20(MciZ)-Asp280(FtsZ) salt bridge, replacing Arg20 by Ala. However, peptide R20A was still active, showing effects similar to wild-type MciZ (Fig. 2D). Replacing Arg20 for Asp (R20D) effectively disabled MciZ activity, so that no effect on cell length or FtsZ:GFP localization was observed (Fig. 2D). This result agrees with the reported lack of interaction (co-purification) of His₆-MciZ-R20D following co-expression with FtsZ (Bisson-Filho *et al.*, 2015). However, in our case the local charge inversion

in R20D could also affect the exogenous MciZ peptide passage through the bacterial envelope prior to interacting with FtsZ in the cytosol. Therefore, we resorted to a more incisive strategy to inhibit MciZ:FtsZ interaction, namely disrupting β -sheet hydrogen bonding between $\beta 9$ of FtsZ and $\beta 2$ of MciZ, without any charge modification. We made different amino acid changes (Fig. 2C): (i) replacing the conserved L12 with a β -sheet breaker residue (Leu12Pro) or with an unnatural D-amino acid (Leu12D-Leu), in order to disrupt the $\beta 2$ strand in the middle and thus the β -sheet hydrogen bond network; (ii) specifically blocking backbone hydrogen bond formation between V10 of MciZ and S296 of FtsZ, or G14 of MciZ and M292 of FtsZ, by replacing these MciZ residues with the corresponding N-methyl-amino acids (V10^mV and G14^mG). We found that MciZ activity was abrogated in each of the resulting analogs, except for V10^mV, which had a weak residual activity requiring higher concentration (40 μM) than the wild type (Fig. 2D). These results showed that single amino acid changes in MciZ, inspired by the crystal structure of the FtsZ:MciZ complex, impair

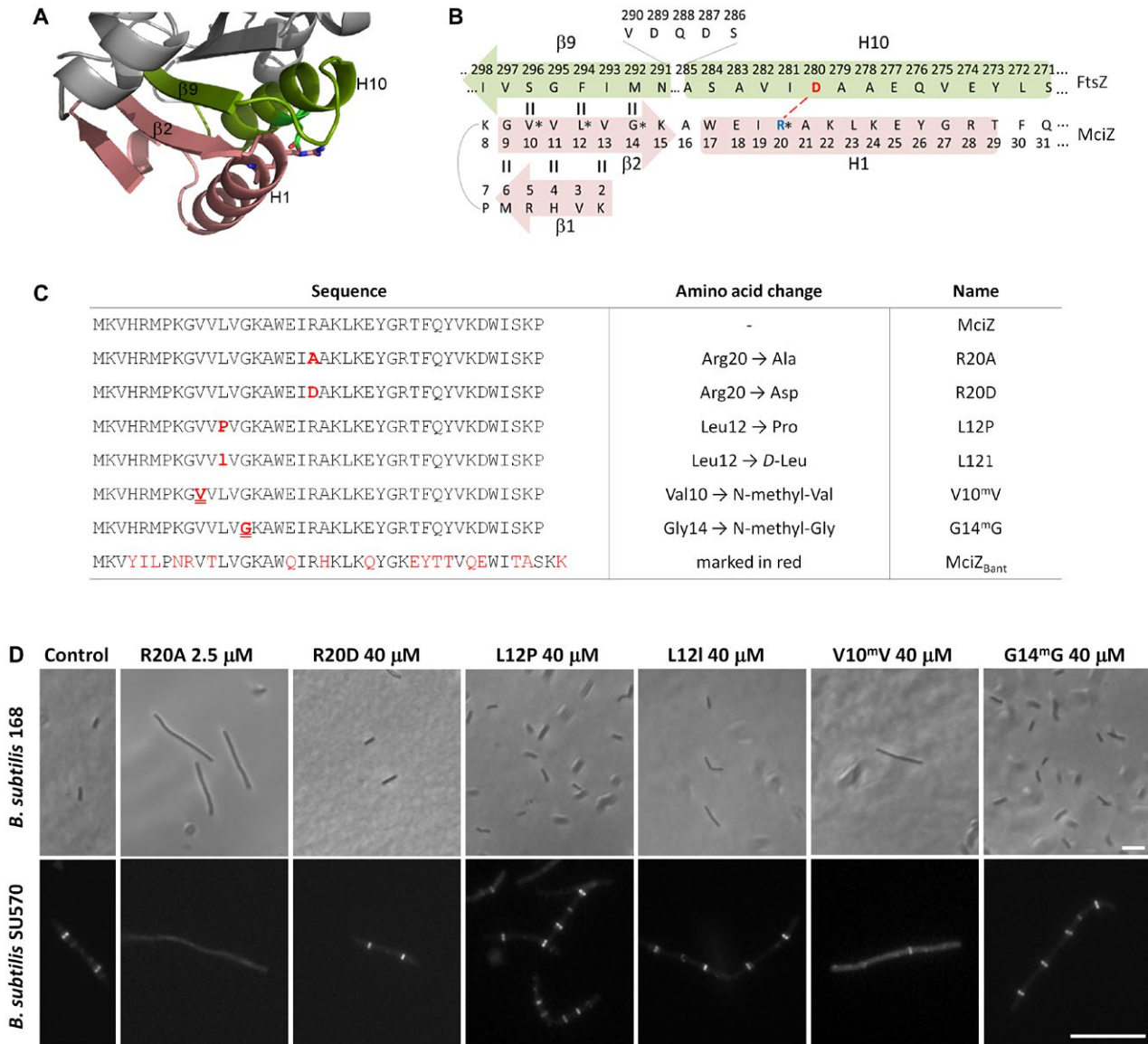


Fig. 2. Synthetic MciZ analogs and their effects on *B. subtilis* cell division and FtsZ subcellular localization.

A. Structure of MciZ (pale red ribbon diagram) in complex with FtsZ (interacting elements in green) (from PDB entry 4U39 molecule A). MciZ β -strands 1 and 2 extend the C-terminal β -sheet of FtsZ. MciZ helix 1 interacts with FtsZ helix 10; residues Arg20 (MciZ) and Asp280 (FtsZ) (in sticks representation) form a salt bridge.

B. Schematic representation of the ionic interactions between MciZ and FtsZ, including the hydrogen bonds formed between MciZ strand β 2 and FtsZ strand β 9. MciZ residues that have been synthetically replaced are marked by asterisks.

C. Peptide sequences of synthetic MciZ analogs employed in this work.

D. *B. subtilis* 168 (phase contrast) or *B. subtilis* SU570 (FtsZ-GFP fluorescence) were incubated with MciZ analogs at the concentrations indicated during 1.5 h and their effects on cell length and FtsZ subcellular localization were analyzed. Representative images of each observed phenotype are shown (scale bars: 10 μ m).

its activity on cell division. They indicated that exogenous MciZ directly interacts with FtsZ in the treated *B. subtilis* cells, although these data did not discard other pathways.

The results of *in vitro* pull-down assays of MciZ and L12P with immobilized His₆-FtsZ supported FtsZ targeting in cells. FtsZ from *B. subtilis* (BsFtsZ) bound MciZ but not its L12P analog (Fig. S2). A truncated version

of BsFtsZ lacking the disordered C-terminal tail (His₆-BsFtsZ Δ Ct, residues 1–315) similarly recognized MciZ. These results are consistent with the lack of activity of L12P on *B. subtilis* and confirm that a single amino acid change is sufficient to disrupt the FtsZ:MciZ interaction; they also demonstrate that the C-terminal tail of BsFtsZ, which is not observed in crystal structures, is not necessary for the interaction with MciZ.

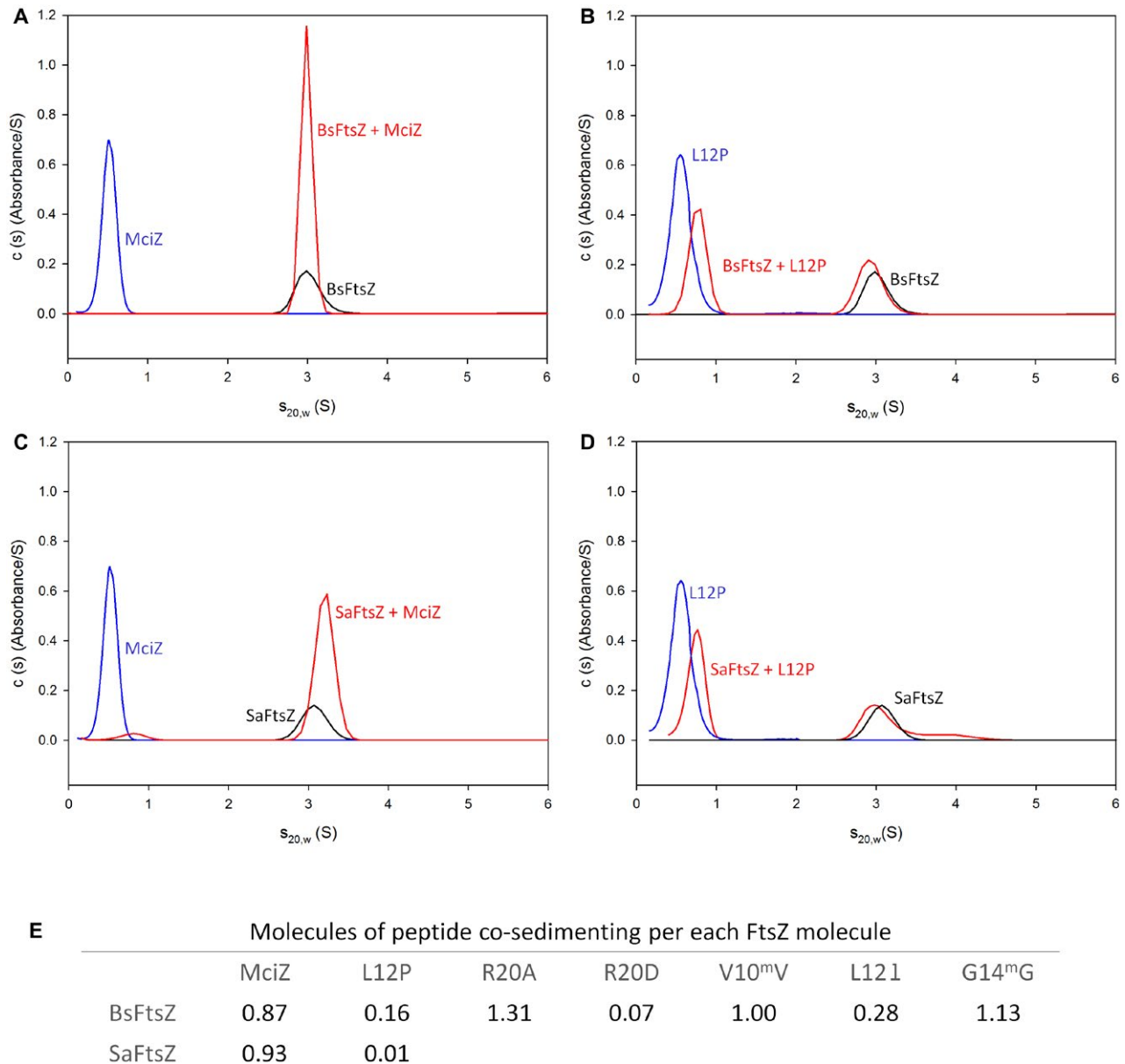


Fig. 3. Binding of MciZ and L12P to FtsZ analyzed with sedimentation velocity AUC.

A–B. Sedimentation coefficient distributions $c(s)$ of 30 μM BsFtsZ (black lines, main peak average $s_{20,w} = 3.0$ S), 30 μM MciZ (A, blue line, 0.5 S), 30 μM L12P (B, blue line, 0.6 S) and the mixtures of 30 μM BsFtsZ with 30 μM MciZ (A, red line, 3.0 S) or with 30 μM L12P (B, red line, 0.8 S and 2.9 S).

C–D. Sedimentation coefficient distribution $c(s)$ of 30 μM SaFtsZ (black line, 3.1 S), 30 μM MciZ (C, blue line, 0.5 S), 30 μM L12P (D, blue line, 0.6 S) and the mixtures of 30 μM SaFtsZ with 30 μM MciZ (C, red line, 0.8 S and 3.2 S) or with 30 μM L12P (D, red line, 0.7 S and 3.0 S). Absorbance data at 293 nm were acquired to monitor peptide sedimentation.

E. The concentrations of sedimenting peptide and FtsZ were calculated to estimate binding stoichiometry (Experimental procedures; see Figure S4 for additional sedimentation coefficient distributions).

Following the reported ability of MciZ to inhibit FtsZ filament assembly by end capping (Bisson-Filho *et al.*, 2015), we confirmed that synthetic MciZ specifically reduces the light scattering increment and the amount of sedimenting polymer upon nucleotide-induced assembly of BsFtsZ under our conditions, in contrast with the inactive peptide L12P that does not affect BsFtsZ assembly (Fig. S3).

Molecular recognition of MciZ peptides by FtsZ from different bacteria

To gain insight into FtsZ:MciZ complex formation in solution, the interaction was first evidenced by co-sedimentation in analytical ultracentrifugation (AUC) experiments. Binding of MciZ to FtsZ was quantified by measuring the MciZ sedimentation velocity profiles in absence and

presence of FtsZ (Fig. 3). BsFtsZ (Fig. 3A and B) and FtsZ from *Staphylococcus aureus* (SaFtsZ; Fig. 3C and D) both sedimented as monomers with $s_{20,w} = 3.0$ and 3.1 S respectively. The lighter MciZ and L12P free peptides sedimented at $s_{20,w} = 0.5$ – 0.6 S. However, in the presence of BsFtsZ or SaFtsZ practically no free MciZ signal was detected but the peptides co-sedimented with FtsZ, in a ratio of 0.9 peptide molecules per FtsZ molecule estimated by subtracting the areas under the 3 S peaks (Fig. 3E); most of the inactive L12P control sedimented as free peptide. These results showed that MciZ specifically forms a 1:1 complex in solution with BsFtsZ and, importantly, they indicated that *B. subtilis* MciZ is also recognized by the homolog SaFtsZ protein. We also analyzed BsFtsZ complex formation with the rest of MciZ analogs by co-sedimentation velocity (Figs. 3E and S4) and the results obtained recapitulated their effects on *B. subtilis* cells, except G14^mG that co-sedimented with FtsZ, which would be compatible with low-affinity binding.

We then characterized the kinetics of interaction between MciZ peptides and FtsZ proteins using bio-layer interferometry (BLI), which revealed different modes of interaction. In a first type of assay, a layer of His₆-BsFtsZ was immobilized on a biosensor tip using the His tag.

This assay showed relatively rapid association of MciZ, R20A and V10^mV, with association rates around $8 \cdot 10^4$ M⁻¹ s⁻¹ and slow dissociation rates around $8 \cdot 10^{-3}$ s⁻¹, giving high affinities with apparent $K_D \approx 0.1$ μM (Fig. 4), compatible with a previous tryptophan fluorescence titration (Bisson-Filho *et al.*, 2015). No binding was observed with the inactive peptide L12P. We then analyzed the interaction between MciZ and different FtsZ species in reverse experiments using a His₆-MciZ immobilized on the biosensor tip. The estimated binding affinities of BsFtsZ and BsFtsZΔCt were similar (Fig. S5), confirming that the C-terminal region of BsFtsZ is not necessary for the interaction with MciZ. Binding of SaFtsZ was about fivefold weaker than BsFtsZ in this BLI assay. The binding and dissociation kinetics were different from the direct experiment and estimated K_D values were one order of magnitude higher, possibly related to the different experimental configuration. The sensorgram with the more distant Gram-negative FtsZ homolog from *Escherichia coli* (EcFtsZ) displayed quite small changes that could not be fitted by a similar binding model (Fig. S5).

Finally, the thermodynamic parameters of MciZ binding to FtsZ were determined by isothermal titration calorimetry (ITC), a reference method to analyze biomolecular

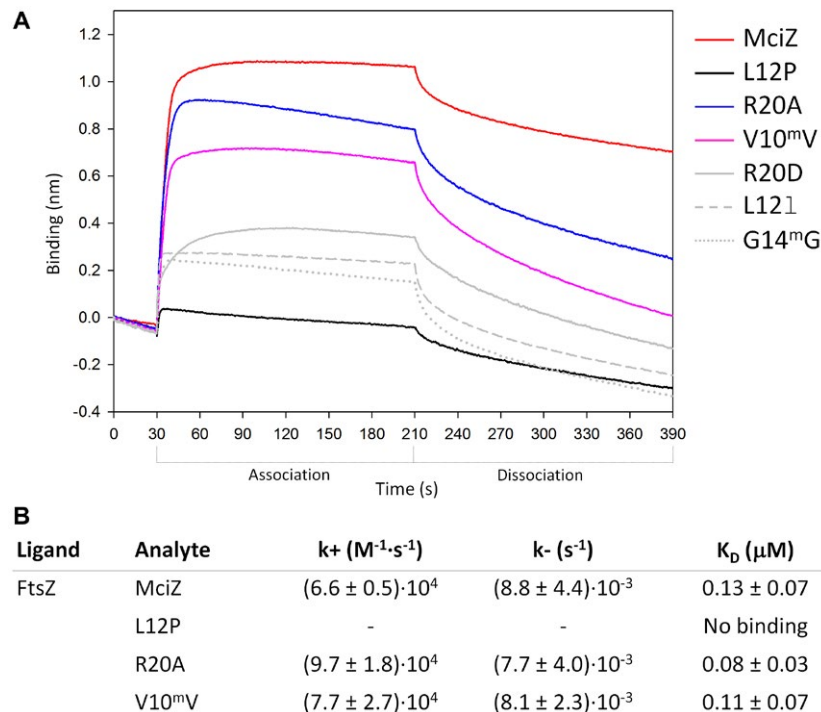


Fig. 4. Interactions of synthetic MciZ peptides with BsFtsZ.

A. Sensorgrams from bio-layer interferometry (BLI) experiments. BsFtsZ (ligand) was immobilized to the tip of the sensor through a His-tag and 2 μM of MciZ or its variants (analytes) were tested for interaction.

B. Kinetic parameters for the interaction of BsFtsZ with synthetic MciZ analogs. The binding of MciZ to FtsZ was analyzed at different concentrations of peptide and the association rate constant (k_+) was determined from the slope of the linear regression line. The dissociation rate constant (k_-) and the equilibrium constant values (K_D ; calculated for a simple binding model) are the average of four independent experiments with MciZ. Two independent experiments were run for the analogs at 2 μM concentration ($R^2 > 0.97$ in all cases). L12P is an inactive peptide. The interactions of R20D, L12I and G14^mG did not adjust to a binding model.

interactions in solution (Freyer and Lewis, 2008). The same buffer, containing 300 mM KCl to shield nonspecific electrostatic interactions, was employed in AUC, BLI and ITC experiments. MciZ binding to FtsZ is endothermic ($\Delta H = 3.3 \text{ kcal mol}^{-1}$), entropy-driven ($-T\Delta S = -12.2 \text{ kcal mol}^{-1}$) (Fig. 5 and Table 1). The observed parameters include any contributions from MciZ peptide folding in addition to binding to FtsZ; they are compatible with a predominant role of hydrophobic interactions. The equilibrium dissociation constant for the interaction of MciZ with BsFtsZ is $K_D = 0.26 \pm 0.15 \text{ }\mu\text{M}$ (Fig. 5A) and the close homolog SaFtsZ has in fact fivefold weaker affinity, $K_D = 1.42 \pm 0.60 \text{ }\mu\text{M}$ (Fig. 5B). The

inactive peptide L12P showed a lack of ITC-detectable binding to BsFtsZ or SaFtsZ, supporting specificity of the MciZ binding. The thermogram of the more distant Gram-negative homolog EcFtsZ titrated with MciZ does not correspond to a binding isotherm, but likely reflects nonspecific interactions (Fig. 5C). The interactions of the other MciZ analogs with BsFtsZ were also measured. The binding affinities of R20A and V10^{mV} (K_D values 0.16 ± 0.1 and $0.18 \pm 0.08 \text{ }\mu\text{M}$ respectively) are similar to MciZ. Binding of G14^{mG} is sevenfold weaker ($K_D = 1.85 \pm 0.62 \text{ }\mu\text{M}$) and the binding of L12I is about 40-fold weaker (Fig. S6 and Table 1). Peptide R20D was found to interact nonspecifically with FtsZ (Fig. S6B).

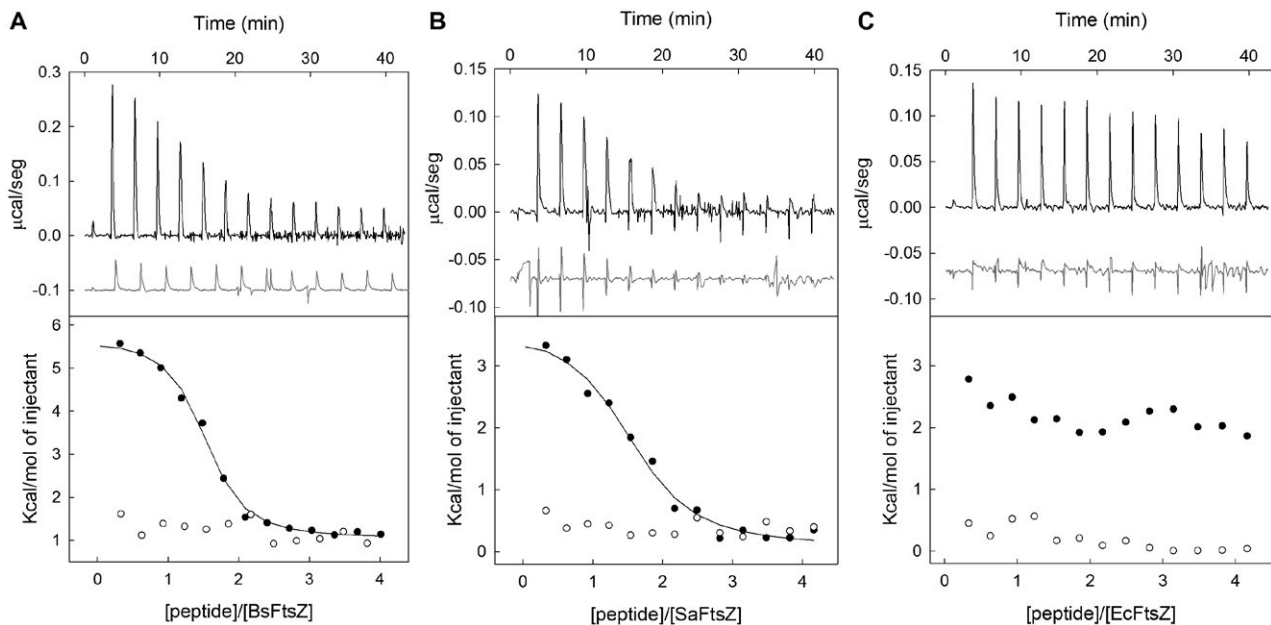


Fig. 5. Calorimetric titrations (ITC) of MciZ interaction with BsFtsZ (A), SaFtsZ (B) and EcFtsZ (C). MciZ, black line and solid circles; L12P control, gray line and empty circles. Each peak (*upper panels*) represents the heat (integrated area) resulting from peptide injection into FtsZ solution. Each point in the *bottom panels* is the heat evolved per mol of injected ligand in the corresponding peak in the *upper panel*. *Solid lines* are the best fits to experimental data. Note that L12P injections in the upper panels are downshifted on the y-axis to facilitate comparison.

Table 1. Energetics of the interactions of MciZ peptides with FtsZ determined by ITC at 25°C.^a

| Peptide ligand and protein | K_D (μM) | ΔG (kcal mol^{-1}) | ΔH (kcal mol^{-1}) | $-T\Delta S$ (kcal mol^{-1}) | n_{app} ^b |
|-------------------------------|-------------------------|---------------------------------------|---------------------------------------|---|-------------------------------|
| MciZ (BsFtsZ) | 0.26 ± 0.15 | -8.88 ± 0.18 | 3.35 ± 0.35 | -12.25 ± 0.02 | 1.5 ± 0.2 |
| MciZ (SaFtsZ) | 1.42 ± 0.60 | -7.98 ± 0.26 | 3.53 ± 0.35 | -11.51 ± 0.02 | 1.5 ± 0.2 |
| R20A (BsFtsZ) | 0.16 ± 0.10 | -9.34 ± 0.06 | 4.06 ± 0.30 | -13.42 ± 0.30 | 1.5 ± 0.1 |
| L12I (BsFtsZ) | 10.8 ± 8.0 | -6.79 ± 0.15 | 6.36 ± 2.80 | -13.09 ± 0.30 | 1.3^c |
| V10 ^{mV} (BsFtsZ) | 0.18 ± 0.08 | -9.23 ± 0.03 | 4.71 ± 0.23 | -13.95 ± 0.15 | 1.3 ± 0.1 |
| G14 ^{mG} (BsFtsZ) | 1.85 ± 0.62 | -7.21 ± 0.15 | 7.07 ± 0.50 | -14.28 ± 0.06 | 0.9 ± 0.1 |
| MciZ _{Bant} (BsFtsZ) | 0.25 ± 0.05 | -9.03 ± 0.14 | 3.14 ± 0.34 | -12.2 ± 0.40 | 1.7 ± 0.2 |

^aValues are average and standard error of at least duplicate experiments. Values for MciZ (BsFtsZ) are an average of five experiments.

^bThe $n > 1$ apparent stoichiometry values may be explained by total MciZ containing inactive (unfolded) free peptide in equilibrium with the active (folded) species for binding to FtsZ.

^cStoichiometry was constrained to $n = 1.3$ in this case.

Interestingly, MciZ from *B. anthracis* (MciZ_{Bant}) binds to BsFtsZ ($K_D = 0.25 \pm 0.05 \mu\text{M}$), with similar affinity and thermodynamic parameters as *B. subtilis* MciZ (Table 1 and Fig. S6F), in spite of the 18 amino acid changes between both MciZs (Fig. 2C).

In summary, the results from the combined AUC, BLI and ITC approaches indicate the entropically driven formation of a MciZ:BsFtsZ high-affinity complex (average $K_D = 0.2 \mu\text{M}$) in solution, whose features are consistent with the specific interactions described in the crystal structure of the core FtsZ:MciZ complex (Bisson-Filho *et al.*, 2015), particularly the β -sheet extension and hydrogen-bonding pattern. The interaction was thus modulated or completely blocked by single amino acid substitutions in five synthetic MciZ analogs, but not by the numerous possibly non-essential substitutions in MciZ_{Bant}. The analog activities on *B. subtilis* (Fig. 2) qualitatively correlate with their different *in vitro* binding affinities to BsFtsZ (Table 1), strongly supporting the notion that cellular FtsZ is being targeted by the exogenous MciZ peptide. Additionally, we have found that MciZ is specifically recognized by purified SaFtsZ and not by EcFtsZ, which points out the potential of MciZ to inhibit FtsZ and cell division in *S. aureus*, as will be described later.

Exogenously added MciZ or induced expression of mciZ impair sporulation and germination in B. subtilis

We next asked whether an excess of MciZ would interfere with the *B. subtilis* sporulation process. MciZ is normally expressed in the mother cell with a peak level 3.5 h after entry into sporulation, which contributes to block the formation of a Z-ring at mid cell (Handler *et al.*, 2008). *B. subtilis* 168 cells, cultured first on a rich medium, were transferred to resuspension medium to induce sporulation (Sterlini and Mandelstam, 1969). Microscopic analysis of the cultures 5 h later revealed the presence of spores in control samples, but slightly filamented cells predominantly lacking spores were observed in samples with 5 μM MciZ (Fig. 6A). These phenotypic changes are consistent with blocking FtsZ assembly both at mid cell and at the prespore region, preventing the asymmetric cell division necessary for spore formation. The presence of MciZ in the sporulation medium caused a reduction of $70 \pm 4\%$ ($n = 3$) in the number of spore colony forming unit (cfu) with respect to the control. As negative control, we repeated the experiment with the inactive peptide L12P and, as expected, the sporulation proceeded normally, the presence of L12P in the sporulation medium only caused a reduction of $5 \pm 1\%$ in the cfu.

To ensure that the inhibitory effect of MciZ on sporulation was not due to potential membrane damage by the synthetic peptide, we examined sporulation in a *B. subtilis*

strain harboring a xylose-inducible copy of *mciZ* (FG1443, Table S5). Control cells of FG1443 growing in resuspension medium sporulated, but treatment with 5 μM MciZ or 1% xylose decreased sporulation, leading to a reduction of $53 \pm 9\%$ and $40 \pm 8\%$, respectively, in the cfu. These results demonstrate that exogenous MciZ or intracellular MciZ expression similarly impair sporulation (Fig. 6A). Division of FG1443 cells was also inhibited by MciZ or xylose (Fig. S7).

We have also tested the effect of MciZ on the germination process. Germination is essential for dormant spores to return to vegetative growth, which is regulated by germination-specific proteins synthesized during spore formation (Paredes-Sabja *et al.*, 2011). To induce germination, heat-activated spores were transferred to germination medium and the optical density of the cultures measured (Fig. 6B). Spores cultured in the absence of MciZ or with 5 μM L12P (inactive peptide) showed similar germination curves; however, exogenously added MciZ completely blocked germination in both strains. Intracellular expressed MciZ impaired germination of the FG1443 strain in a milder way than exogenous MciZ, possibly due to differences in intracellular MciZ concentration. Our results demonstrate that excess MciZ can impair different modes of *B. subtilis* reproduction since it is not only able to arrest vegetative growth by targeting FtsZ, but it can also inhibit sporulation and germination, which are crucial for dissemination and survival.

Inhibition of cell division in different Bacillus species by synthetic B. subtilis and B. anthracis MciZ

Conserved genomic sequences encoding homologs of the *B. subtilis* MciZ developmental regulator spread across *Bacillus* species, suggesting that MciZ confers a fitness advantage facilitating sporulation. However, MciZ is not essential for sporulation, probably due to redundancy with other factors preventing cytokinesis in the mother cell (Handler *et al.*, 2008). A phylogenetic tree constructed with the MciZ sequences $\geq 55\%$ identical to *B. subtilis* MciZ is shown in Fig. 7A. In addition to potential MciZs from *Bacillus spp.*, a hypothetical 56-amino acid homolog with 46% identity was found in *Clostridium ultunense* (GenBank: CCQ95631.1). Although there is substantial diversity between *Bacilli* and *Clostridia* sporulation processes (Paredes-Sabja *et al.*, 2014), in both cases the decision to enter sporulation falls on the transcriptional regulator Spo0A (Steiner *et al.*, 2011; Higgins and Dworkin, 2012) and on the activation cascade of sporulation-specific RNA polymerase sigma factors (Haraldsen and Sonenshein, 2003; de Hoon *et al.*, 2010); therefore, a functional MciZ would make sense in *Clostridium*.

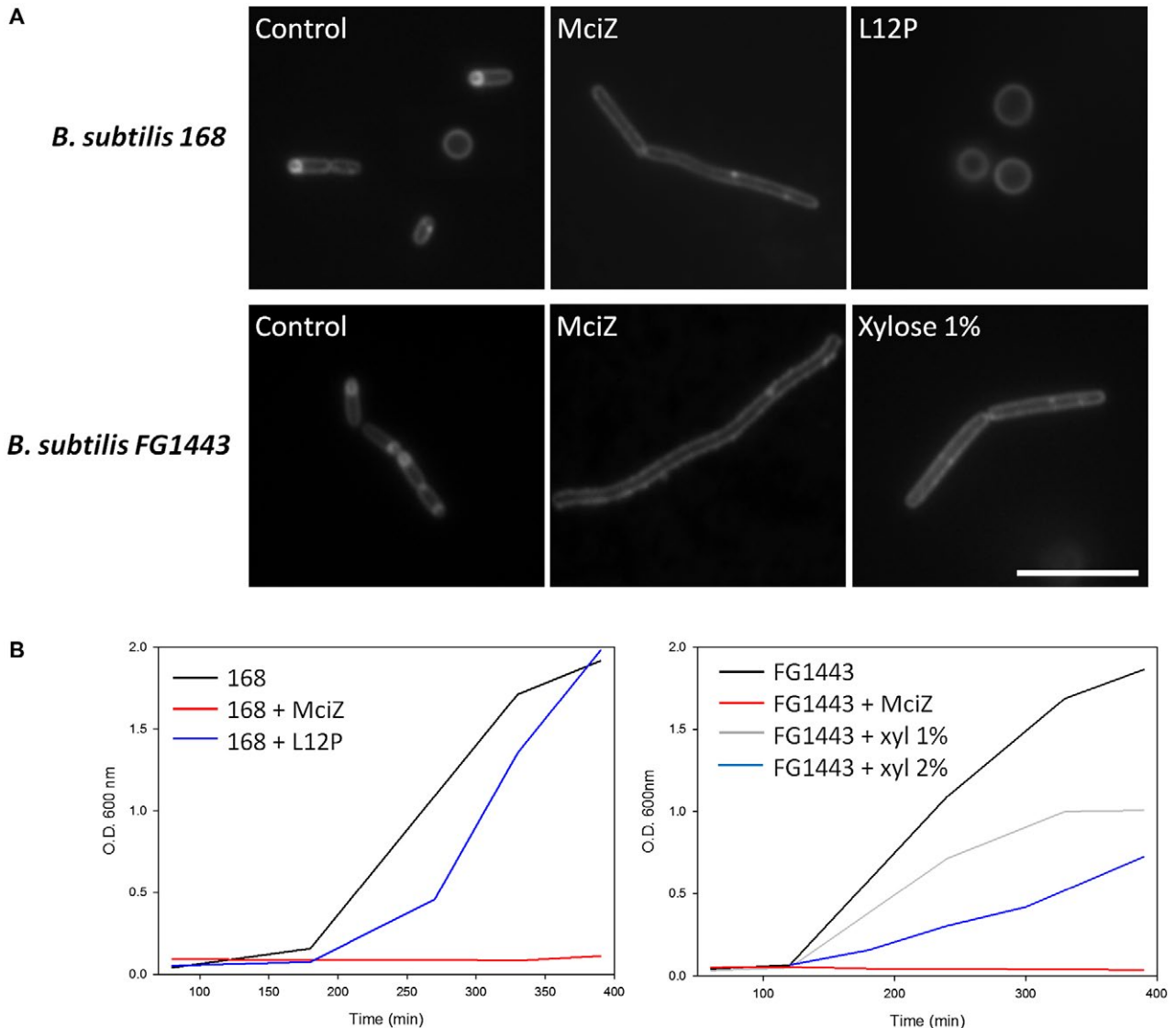


Fig. 6. Effects of exogenous and endogenous MciZ on sporulation and germination.

A. *B. subtilis* cells were stained with the membrane dye FM4-64 and examined by fluorescence microscopy, 5 h after inducing sporulation. *B. subtilis* 168 was grown in sporulation medium without (control) or with 5 μ M MciZ or 5 μ M L12P inactive analog, as indicated; representative images of treated cells or spores are shown in each case. *B. subtilis* strain FG1443 (*amyE::Pxyl-mciZ*) – which harbors a xylose-inducible copy of *mciZ* – was grown in sporulation medium without (control) or with 5 μ M MciZ or 1% xylose. Scale bar: 10 μ m.

B. Left: germination curves of *B. subtilis* 168 in the absence or presence of MciZ or L12P (5 μ M) added to the culture medium. Right: Germination curves of *B. subtilis* FG1443, with MciZ (5 μ M) or xylose (1–2% w/v).

To explore the degree of specificity of MciZ action on different *Bacillus* species, we compared the inhibition of cell division by exogenous MciZ in two relatively distant *Bacillus* clades: the closely related group of *B. subtilis*, *B. amyloliquefaciens* and *B. licheniformis*, and the branch of the insecticidal *B. thuringiensis*, the food pathogen *B. cereus* and the anthrax agent *B. anthracis*, also very closely related among them (Fig. 7A). In order to permit comparisons in both directions, in addition to *B. subtilis* MciZ we also employed MciZ from *B. anthracis* (Fig. 2C). We cultured cells of the different *Bacillus* spp. in the

presence of increasing nontoxic concentrations of each peptide and quantified their effects on division (Fig. 7B, raw data in Fig. S8, see Table S3 for length measurements, Table S4 for MDP). *B. subtilis* was the more sensitive species: 2.5 μ M MciZ or MciZ_{Bant} led to a comparable 6–7 fold increase in cell length in agreement with their equal affinities for BsFtsZ (Table 1). Supportingly, MciZ_{Bant} inhibited BsFtsZ *in vitro* assembly similarly to MciZ (Fig. S3).

A higher concentration of MciZ (10 μ M) was required for similar effects on the close *B. amyloliquefaciens* and *B. licheniformis*, which were less sensitive to MciZ_{Bant}

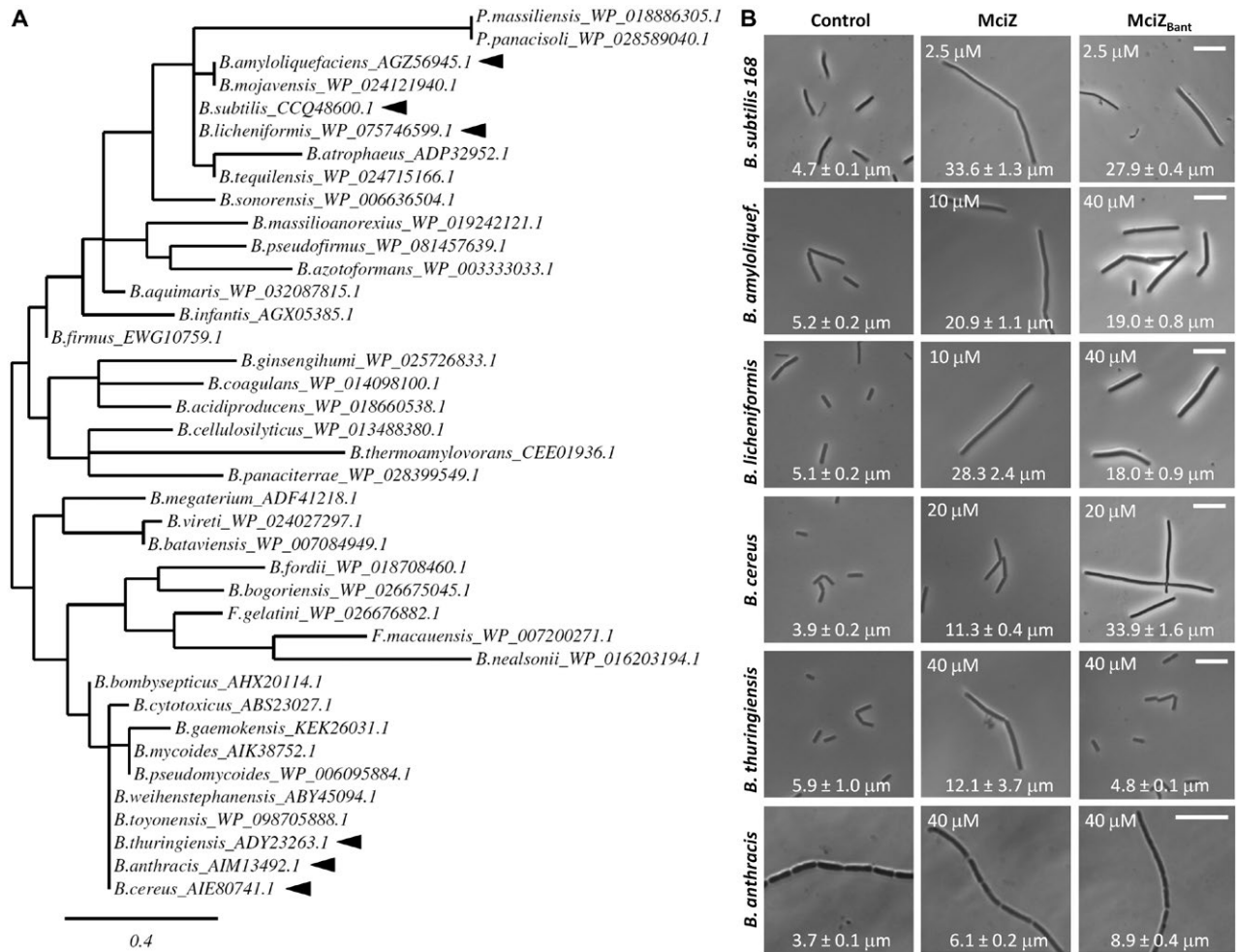


Fig. 7. Effect of synthetic *B. subtilis* and *B. anthracis* MciZ on phylogenetically related *Bacillus* species.

A. Phylogenetic tree of *Bacillus* species based on MciZ protein sequences. Sequences were obtained from GenBank and NCBI. Accession numbers for each sequence are shown. Branch length is proportional to estimated phylogenetic distance, in amino acid substitutions per site. Arrowheads: *Bacillus* species selected for cellular studies.

B. Cells of *Bacillus* spp. were incubated during 3 h with MciZ or MciZ_{Bant} and their effects on cell length were analyzed under the microscope using phase contrast and quantified by measuring cell length in FM4-64 membrane stained cells. Representative examples of each observed phenotype are shown (scale bars: 10 μm). The peptide concentrations employed and mean cell lengths are indicated in each case.

(40 μM). *B. thuringiensis-cereus-anthraxis* were less sensitive than the *B. subtilis* group to MciZ and they showed no selectivity for MciZ_{Bant}, which lacked effect on *B. thuringiensis*. MciZ and MciZ_{Bant} (40 μM) had small but significant effects on *B. anthracis* cell division (~twofold increased cell length).

We concluded from these results that the specificity of MciZ action in *Bacillus* is low, which is compatible with the conservation of practically identical sequences in the MciZ binding elements of FtsZ in the six species examined (Fig. S9). The different sensitivities to MciZ may thus be speculated to be related to differences in peptide permeability of their cell envelopes. On a practical side, the effects of MciZ on pathogenic *B. cereus*, *B. thuringiensis* and *B. anthracis* suggest its potential use to design new

specific antibacterial inhibitors. The infectious agent of anthrax is the dormant endospore and we have observed that MciZ or MciZ_{Bant} added to the medium impair sporulation of *B. cereus* (reduction of 36 ± 8% and 66 ± 5%, respectively, in the cfu after 5 h of sporulation), the closer relative of *B. anthracis*, although no effect on *B. cereus* germination was observed (Fig. S10).

Inhibition of *S. aureus* cell division by intracellular expression of *B. subtilis* MciZ

The results obtained with AUC, BLI and ITC demonstrated that purified SaFtsZ recognizes MciZ from *B. subtilis*, consistent with small differences in the MciZ binding region of FtsZ between BsFtsZ and SaFtsZ

exogenously added or endogenously inducible MciZ (strain BL21+pAB50, Table S5), which is consistent with the lack of specific binding of MciZ to EcFtsZ that had been observed *in vitro*. These results may be explained by the weak conservation of the MciZ binding residues in EcFtsZ (Fig. 8A). Our results also suggest the design of MciZ-based peptide antibacterials against *S. aureus*. One possibility would be the use of vectors such as cell-penetrating peptides (Copolovici *et al.*, 2014), an approach that has been broadly explored for drug delivery to tumor cells (Wang and Wang, 2012) and less often against infectious diseases (de la Torre *et al.*, 2014). As a preliminary test, we tried synthetic MciZ fused to a N-terminal cell-penetrating Tat sequence that enhanced filamentation and toxicity on *B. subtilis*, but lacked effect on *S. aureus* (40 μ M Tat-MciZ); additional possibilities remain to be studied.

Conclusion

We have shown that exogenous MciZ peptides inhibit *B. subtilis* cell division, sporulation and germination, and have analyzed in detail MciZ molecular recognition by different FtsZ. The cell division inhibitory activity of synthetic MciZ extends to pathogenic *B. cereus* – *B. anthracis*. Given the complexity of the sporulation process, where many factors are involved, we cannot discard the possibility that another cellular mechanism or receptor, in addition to direct inhibition of FtsZ assembly, might explain the selective action of MciZ in *Bacillus*. However, based on the results obtained with *S. aureus*, a nonspore-forming pathogen, we propose that entry or expression of *B. subtilis* MciZ within bacterial cells is sufficient to inhibit division as long as the MciZ key recognition residues in helix H10-strand β 9 of FtsZ are conserved. Our results suggest the possibility of designing MciZ-based peptide antibacterial agents targeting cell division.

Experimental procedures

Peptides

MciZ and the analogs shown in Fig. 2C were assembled on either Prelude (Gyros Protein Technologies, Tucson, AZ) or microwave-assisted Liberty Blue (CEM Corp., Matthews, NC) synthesizers, using ChemMatrix (PCAS Biomatrix Inc., Saint-Jean-sur-Richelieu, Quebec, Canada) or 2-chlorotriyl chloride (Iris Biotech GmbH, Marktredwitz, Germany) resins, respectively, and optimized Fmoc solid-phase synthesis protocols, including the N-methyl substituted Fmoc-MeVal and Fmoc-N-MeGly residues in V10^MV and G14^MG respectively. For coupling onto MeVal and MeGly residues the synthesis was switched to manual mode, the respective peptide resins were first deprotected with piperidine/

dimethylformamide (DMF) (20% v/v, 2 \times 10 min) and piperidine/1,8-diazabicyclo(5.4.0)undec-7-ene/toluene/DMF (5:5:20:70, v/v; 2 \times 5 min), then the incoming Fmoc-Gly⁹ and Fmoc-Val¹³ were, respectively, added to the resin in fivefold molar excess, along with 7-azabenzotriazol-1-yloxy)tripyrrolidinophosphonium hexafluorophosphate (PyAOP) and N, N-diisopropylethylamine (5- and 10-fold molar excess respectively), in DMF as solvent and allowed to react for 1 h with intermittent manual stirring. An additional (2.5 molar excess) amount of PyAOP was next added and the mixture stirred for another 60 min. Synthesis was then resumed in automated mode for the remaining residues of each sequence.

After deprotection and cleavage with trifluoroacetic acid/H₂O/triisopropylsilane (95:2.5:2.5 v/v, 90 min, r.t.), the peptides were isolated by precipitation with cold ethyl ether, reconstituted in water and lyophilized. Preparative reverse phase HPLC purification yielded the target peptides in >95% homogeneity, with mass spectra consistent with the expected composition. Additional peptides (not listed on Fig. 2C) included versions of both MciZ and R20A elongated at the N-terminus with the Tat(48-60) (GRKKRRQRRPPQ) cell-penetrating sequence.

Peptide stock solutions (5 mM) were prepared in distilled water before use. Concentration was measured spectrophotometrically using an extinction coefficient of 13,980 M⁻¹ cm⁻¹ at 280 nm, calculated from the amino acid sequence. PC190723 was synthesized as previously described (Andreu *et al.*, 2010) and stock solutions prepared in dimethyl sulfoxide, whose residual concentration in treated cultures and controls was less than 0.5%.

Bacterial strains, plasmids and microscopy

All strains and plasmids used in this work are listed in Table S5. *Bacillus* spp, except *B. anthracis*, were grown in cation-adjusted Mueller-Hinton broth (CAMHB; Becton, Dickinson and Company) at 37°C. *B. anthracis* was grown in Nutrient Broth medium (beef extract 5 g L⁻¹, peptone 10 g L⁻¹, NaCl 5 g L⁻¹, pH 7.2) and manipulated at the Neglected and Emerging Diseases Unit of the VISAVET Health Surveillance Centre (Universidad Complutense de Madrid, Spain). *S. aureus* RN4220 was grown in Trypticasein Soy Broth (TSB, Eur Pharm, Pronadisa) at 37°C. MIC values were determined by a broth macrodilution method as described (Artola *et al.*, 2015).

To construct plasmid pCN51-P_{cad}-mciZ, a 124 bp fragment containing the *mciZ* open reading frame was amplified using primers mciZ-BamHI (5'-AAGGATCCATGAAAGTGCACCGCAT-3') and mciZ-EcoRI (5'-AAGAATTC-TTATGGCTTTGAGATCCAATC-3'). The PCR product was digested with BamHI and EcoRI (sites underlined in primer sequences above) and cloned into pCN51, cut with the same enzymes. Expression of *mciZ* was induced by 2.5 μ M CdCl₂. Antibiotics were used at the following concentrations: chloramphenicol, 5 μ g mL⁻¹; spectinomycin, 100 μ g mL⁻¹; erythromycin, 10 μ g mL⁻¹; kanamycin, 50 μ g mL⁻¹; ampicillin, 100 μ g mL⁻¹. Microscopy assays were performed as previously described (Araujo-Bazan *et al.*, 2016), except *B. anthracis* that was subjected to Gram staining. Line profiles were drawn on cell membranes stained with FM4-64 to measure cell

length, distinguishing elongation from potential cell chaining, using the analysis tools of Wasabi software (Hamamatsu).

Sporulation and germination assays

Bacillus subtilis or *B. cereus* cells were grown in CAMBH at 37°C, inoculated at an OD₆₀₀ of 0.05 from an overnight culture grown in the same medium. When the culture reached OD₆₀₀ 0.14, sporulation was induced by transferring cells to the resuspension medium of Sterlini and Mandelstam (Sterlini and Mandelstam, 1969). After 24 h in sporulation medium spores were harvested (3,000 g, 15 min, 4°C) and resuspended in 50 mM potassium phosphate buffer (pH 8.0) with phenylmethylsulfonyl fluoride (1 mM), lysozyme (10 mg mL⁻¹), DNase-I (25 µg mL⁻¹) and RNase (25 µg mL⁻¹) and samples were incubated 60 min at 30°C to eliminate possible vegetative cells (Seydlova and Svobodova, 2012). The intact spores were sedimented by centrifugation (3,000 g, 10 min, 4°C), washed three times with distilled water and stored at 4°C. All spores used for germination were first heat-activated in distilled water for 30 min at 70°C. Germination of heat-activated spores was triggered in CAMHB medium supplemented with 10 mM L-asparagine, 10 mM glucose, 1 mM fructose and 1 mM potassium chloride (Pandey *et al.*, 2013). To quantify sporulation efficiency, 5 h sporulating cultures were plated following spore collection, elimination of vegetative cells and heat-activating spores as above. CFU was determined by counting colonies after 24 h at 37°C.

Protein purification

BsFtsZ, BsFtsZCt (Huecas *et al.*, 2017), SaFtsZ and EcFtsZ (Artola *et al.*, 2017) were purified as described. His₆-BsFtsZ and His₆-BsFtsZΔCt were purified as BsFtsZ and BsFtsZΔCt, respectively, but without the His-tag cleavage step. BsFtsZ polymerization was monitored by light scattering and sedimentation in 50 mM Hepes-KOH, 300 mM KCl, 1 mM EDTA, 10 mM MgCl₂, 100 µM GMPCPP, pH 6.8 at 25°C as described (Ruiz-Avila *et al.*, 2013).

His₆-MciZ for BLI assays was expressed in *E. coli* BL21 cells transformed with plasmid pAB50. The expression was induced with 1 mM isopropyl-β-D-thiogalactopyranoside. After 3 h of induction at 37°C cells were harvested by centrifugation and the pellet was resuspended in 50 mM Hepes-KOH, 300 mM KCl, 1 mM EDTA, pH 6.8, supplemented with 0.1 mM GDP. Cells were lysed by sonication, the lysate was cleared by centrifugation at 20,000 g for 20 min at 4°C, and directly applied to the biosensor.

Pull-down assay

For *in vitro* MciZ binding assays, 10 µM purified His₆-BsFtsZ or His₆-BsFtsZΔCt was incubated with 25 µL of nickel NTA agarose beads (ABT) for 1 h at 4°C, in binding buffer (50 mM NaH₂PO₄, 300 mM NaCl, 10 mM imidazole, pH 8.0). The beads were washed 3 times at 500 g with washing buffer (50 mM NaH₂PO₄, 300 mM NaCl, 20 mM imidazole, pH 8.0) and washed beads, with His₆-BsFtsZ or His₆-BsFtsZΔCt bound, were incubated with 10 µM MciZ or L12P in binding buffer for 1 h at 4°C. The beads were then pelleted down

and the not retained material was collected. Bound proteins were eluted with elution buffer (50 mM NaH₂PO₄, 300 mM NaCl, 250 mM imidazole, pH 8.0). Eluted and not retained proteins were separated by SDS-PAGE and stained using Coomassie blue.

Analytical ultracentrifugation

Sedimentation velocity experiments were made in a Beckman Optima XL-I analytical ultracentrifuge equipped with interference and absorbance optics providing a linear response in the concentration range employed, using an An50/Ti rotor with 12 mm double-sector centerpieces at 45,000 rpm, 25°C. Differential sedimentation coefficient distributions, c(s), were calculated with SEDFIT (Schuck *et al.*, 2002). The weight average sedimentation coefficient values measured in buffer at 25°C were corrected to H₂O at 20°C, s_{20,w}. Ligand to protein binding was measured by co-sedimentation analysis (Barbier *et al.*, 2010; Ruiz-Avila *et al.*, 2013; with modifications). The FtsZ protein concentration (area under the 3 S peak) was measured by refractive index increment (3.25 fringes per mg mL⁻¹ protein, to which the lower mass peptide ligand contributes very little). The MciZ peptide was measured by absorption at 293 nm (subtracting the small contribution of the proteins employed that lack Trp residues and absorb less than MciZ at this wavelength). The area under the MciZ peak co-sedimenting with FtsZ (3 S) in the c(S) distribution of the peptide was employed to calculate the concentration of peptide bound to the protein (using a peptide absorptivity of 5275 M⁻¹ cm⁻¹ at 293 nm, determined from initial scans at 3,000 rpm). AUC experiments were done in 50 mM Hepes-KOH, 300 mM KCl, 1 mM EDTA, pH 6.8, supplemented with 0.1 mM GDP (HK300 buffer).

Bio-layer interferometry

The interaction between peptides and BsFtsZ was analyzed using a single-channel BLItz system with Ni-NTA biosensors (ForteBio, Menlo Park, CA, USA). His₆-BsFtsZ was immobilized through the His-tag on the sensors, at a final concentration of 100 µg mL⁻¹ in HK300 buffer. Experiments were performed at ~22°C and a shake speed of 2,200 rpm, with baseline for 30 s followed by an association phase (experimental sample) for 180 s and a dissociation phase (buffer alone) for 180 s. The interacting peptides in the same buffer were added to generate the sensorgrams. The best fit association and dissociation rate constants were determined using the BLItz Pro software and Sigma Plot (Systat Software). The interaction between MciZ and different species of FtsZ was analyzed in reverse experiments in which His₆-MciZ was immobilized on the biosensor tip. The interacting proteins (BsFtsZ, BsFtsZΔCt, SaFtsZ or EcFtsZ, 100 µg mL⁻¹) were added in the same buffer.

Isothermal titration calorimetry

ITC measurements were performed using a MicroCal PEAQ-ITC calorimeter (Malvern). The sample cell

(0.2 mL) was loaded with 10 μ M FtsZ, equilibrated in the experimental buffer with a Fast Desalting Column HR 10/10 (Pharmacia Biotech), and the syringe was loaded with the peptide at a concentration comprised between 200 and 250 μ M. Experiments were performed in HK300 buffer. Concentrated stock solutions of peptide in water were diluted to the experimental concentrations in buffer. An identical small proportion of water was introduced in the protein sample. As a control experiment, the individual dilution heats for the syringe reactant were determined by carrying out identical injections of the reactant into the sample cell with buffer. Controls without peptide and buffer in buffer controls were also run. A total of 13 injections of 3 μ L were sequentially mixed into the sample cell with 180 s spacing. The electrical power required to maintain the reaction cell at constant temperature after each injection was recorded as a function of time, generating the thermograms shown. Binding isotherms were fitted to a single type of site model using the MicroCal PEAQ-ITC Analysis software.

Phylogenetic tree

Phylogenetic analysis was performed on the Phylogeny.fr platform (<http://www.phylogeny.fr/>) (Dereeper *et al.*, 2008). Sequences were aligned with MUSCLE (v3.8.31) configured for highest accuracy. The phylogenetic tree was reconstructed using the maximum likelihood method implemented in the PhyML program (v3.1/3.0 aLRT). The WAG substitution model was selected assuming an estimated proportion of invariant sites (of 0.084) and 4 gamma-distributed rate categories to account for rate heterogeneity across sites. The gamma shape parameter was estimated directly from the data ($\gamma = 2.455$). Reliability for internal branch was assessed using the aLRT test (SH-Like). Graphical representation and edition of the phylogenetic tree were performed with TreeDyn (v198.3).

Acknowledgements

We thank Dr. M. A. Jimenez, Institute of Physical Chemistry Rocasolano (IQFR), CSIC Madrid, for valuable help designing MciZ peptide analogs and discussions; Dr. M. Menéndez, IQFR, CSIC Madrid, for advice on ITC and discussions; Drs. M.A. Peñalva and M. Espinosa, Centro de Investigaciones Biológicas, for critical reading of the manuscript. We especially thank Dr. Nerea García and Irene Martínez, Neglected and Emerging Diseases Unit of the VISAVET Health Surveillance Centre (Universidad Complutense de Madrid, Spain), for *B. anthracis* growth and manipulation. We thank Dr. F. Gueiros-Filho, University of Sao Paulo, Brasil; Dr. A. Bisson-Filho, Harvard University, USA; Dr. E. Harry, ithree institute, University of Technology, Australia; and Dr. I. Lasa, Universidad Pública de Navarra, Spain, for kindly providing strains and plasmids. We thank David Juan, Centro de Investigaciones Biológicas, for FtsZ protein purification, and the Medicinal Chemistry laboratory (Dr. M. L. López-Rodríguez), Universidad Complutense de Madrid, Spain, for synthesizing PC190723. This work was

funded by MINECO grants BFU 2014-51823-R to JMA and AGL2014-52395-C2 to DA.

Author contributions

L.A-B., D.A. and J.M.A. designed experiments, L.A-B. performed the experiments, S.H. performed the ITC experiments, J.V. synthesized the peptides, L.A-B and J.M.A. wrote the manuscript with input from the other authors.

References

- Adams, D.W., Wu, L.J. and Errington, J. (2016) A benzamide-dependent ftsZ mutant reveals residues crucial for Z-ring assembly. *Molecular Microbiology*, **99**, 1028–1042.
- Anderson, D.E., Gueiros-Filho, F.J. and Erickson, H.P. (2004) Assembly dynamics of FtsZ rings in *Bacillus subtilis* and *Escherichia coli* and effects of FtsZ-regulating proteins. *Journal of Bacteriology*, **186**, 5775–5781.
- Andreu, J.M., Schaffner-Barbero, C., Huecas, S., Alonso, D., Lopez-Rodriguez, M.L., Ruiz-Avila, L.B., *et al.* (2010) The antibacterial cell division inhibitor PC190723 is an FtsZ polymer-stabilizing agent that induces filament assembly and condensation. *Journal of Biological Chemistry*, **285**, 14239–14246.
- Araujo-Bazan, L., Ruiz-Avila, L.B., Andreu, D., Huecas, S. and Andreu, J.M. (2016) Cytological profile of antibacterial FtsZ inhibitors and synthetic peptide MciZ. *Frontiers in Microbiology*, **7**, 1558.
- Arjes, H.A., Kriel, A., Sorto, N.A., Shaw, J.T., Wang, J.D. and Levin, P.A. (2014) Failsafe mechanisms couple division and DNA replication in bacteria. *Current Biology*, **24**, 2149–2155.
- Artola, M., Ruiz-Avila, L.B., Vergonos, A., Huecas, S., Araujo-Bazan, L., Martin-Fontecha, M., *et al.* (2015) Effective GTP-replacing FtsZ inhibitors and antibacterial mechanism of action. *ACS Chemical Biology*, **10**, 834–843.
- Artola, M., Ruiz-Avila, L.B., Ramirez-Aportela, E., Martinez, R.F., Araujo-Bazan, L., Vazquez-Villa, H., *et al.* (2017) The structural assembly switch of cell division protein FtsZ probed with fluorescent allosteric inhibitors. *Chemical Science*, **8**, 1525–1534.
- Barbier, P., Dorleans, A., Devred, F., Sanz, L., Allegro, D., Alfonso, C., *et al.* (2010) Stathmin and interfacial microtubule inhibitors recognize a naturally curved conformation of tubulin dimers. *Journal of Biological Chemistry*, **285**, 31672–31681.
- Bi, E.F. and Lutkenhaus, J. (1991) FtsZ ring structure associated with division in *Escherichia coli*. *Nature*, **354**, 161–164.
- Bisson-Filho, A.W., Discola, K.F., Castellen, P., Blasios, V., Martins, A., Sforca, M.L., *et al.* (2015) FtsZ filament capping by MciZ, a developmental regulator of bacterial division. *Proceedings of the National Academy of Sciences of the United States of America*, **112**, E2130–E2138.
- Bisson-Filho, A.W., Hsu, Y.P., Squyres, G.R., Kuru, E., Wu, F., Jukes, C., *et al.* (2017) Treadmilling by FtsZ filaments

- drives peptidoglycan synthesis and bacterial cell division. *Science*, **355**, 739–743.
- Buske, P.J., Mittal, A., Pappu, R.V. and Levin, P.A. (2015) An intrinsically disordered linker plays a critical role in bacterial cell division. *Seminars in Cell & Developmental Biology*, **37**, 3–10.
- Copolovici, D.M., Langel, K., Eriste, E. and Langel, U. (2014) Cell-penetrating peptides: design, synthesis, and applications. *ACS Nano*, **8**, 1972–1994.
- Cordell, S.C., Robinson, E.J. and Lowe, J. (2003) Crystal structure of the SOS cell division inhibitor Sula and in complex with FtsZ. *Proceedings of the National Academy of Sciences of the United States of America*, **100**, 7889–7894.
- de Hoon, M.J.L., Eichenberger, P. and Vitkup, D. (2010) Hierarchical evolution of the bacterial sporulation network. *Current Biology*, **20**, R735–R745.
- de la Torre, B.G., Hornillos, V., Luque-Ortega, J.R., Abengozar, M.A., Amat-Guerri, F., Acuna, A.U., *et al.* (2014) A BODIPY-embedding miltefosine analog linked to cell-penetrating Tat(48–60) peptide favors intracellular delivery and visualization of the antiparasitic drug. *Amino Acids*, **46**, 1047–1058.
- den Blaauwen, T., Andreu, J.M. and Monasterio, O. (2014) Bacterial cell division proteins as antibiotic targets. *Bioorganic Chemistry*, **55**, 27–38.
- den Blaauwen, T., Hamoen, L.W. and Levin, P.A. (2017) The divisome at 25: the road ahead. *Current Opinion in Microbiology*, **36**, 85–94.
- Dereeper, A., Guignon, V., Blanc, G., Audic, S., Buffet, S., Chevenet, F., *et al.* (2008) Phylogeny.fr: robust phylogenetic analysis for the non-specialist. *Nucleic Acids Research*, **36**, W465–W469.
- Du, S. and Lutkenhaus, J. (2017) Assembly and activation of the *Escherichia coli* divisome. *Molecular Microbiology*, **105**, 177–187.
- Egan, A.J., Cleverley, R.M., Peters, K., Lewis, R.J. and Vollmer, W. (2017) Regulation of bacterial cell wall growth. *FEBS Journal*, **284**, 851–867.
- Elsen, N.L., Lu, J., Parthasarathy, G., Reid, J.C., Sharma, S., Soisson, S.M., *et al.* (2012) Mechanism of action of the cell-division inhibitor PC190723: modulation of FtsZ assembly cooperativity. *Journal of the American Chemical Society*, **134**, 12342–12345.
- Errington, J. (2003) Regulation of endospore formation in *Bacillus subtilis*. *Nature Reviews Microbiology*, **1**, 117–126.
- Freyer, M.W. and Lewis, E.A. (2008) Isothermal titration calorimetry: experimental design, data analysis, and probing macromolecule/ligand binding and kinetic interactions. *Methods in Cell Biology*, **84**, 79–113.
- Fujita, J., Maeda, Y., Mizohata, E., Inoue, T., Kaul, M., Parhi, A.K., *et al.* (2017) Structural flexibility of an inhibitor overcomes drug resistance mutations in *Staphylococcus aureus* FtsZ. *ACS Chemical Biology*, **12**, 1947–1955.
- Haeusser, D.P. and Margolin, W. (2016) Splitsville: structural and functional insights into the dynamic bacterial Z ring. *Nature Reviews Microbiology*, **14**, 305–319.
- Handler, A.A., Lim, J.E. and Losick, R. (2008) Peptide inhibitor of cytokinesis during sporulation in *Bacillus subtilis*. *Molecular Microbiology*, **68**, 588–599.
- Haraldsen, J.D. and Sonenshein, A.L. (2003) Efficient sporulation in *Clostridium difficile* requires disruption of the sigmaK gene. *Molecular Microbiology*, **48**, 811–821.
- Haydon, D.J., Stokes, N.R., Ure, R., Galbraith, G., Bennett, J.M., Brown, D.R., *et al.* (2008) An inhibitor of FtsZ with potent and selective anti-staphylococcal activity. *Science*, **321**, 1673–1675.
- Higgins, D. and Dworkin, J. (2012) Recent progress in *Bacillus subtilis* sporulation. *FEMS Microbiology Reviews*, **36**, 131–148.
- Huecas, S., Ramirez-Aportela, E., Vergonos, A., Nunez-Ramirez, R., Llorca, O., Diaz, J.F., *et al.* (2017) Self-organization of FtsZ polymers in solution reveals spacer role of the disordered C-terminal tail. *Biophysical Journal*, **113**, 1831–1844.
- Kaul, M., Mark, L., Parhi, A.K., LaVoie, E.J. and Pilch, D.S. (2016) Combining the FtsZ-targeting prodrug TXA709 and the cephalosporin cefdinir confers synergy and reduces the frequency of resistance in methicillin-resistant *Staphylococcus aureus*. *Antimicrobial Agents and Chemotherapy*, **60**, 4290–4296.
- Kim, S.J., Chang, J. and Singh, M. (2015) Peptidoglycan architecture of Gram-positive bacteria by solid-state NMR. *Biochimica et Biophysica Acta*, **1848**, 350–362.
- Levin, P.A. and Losick, R. (1996) Transcription factor Spo0A switches the localization of the cell division protein FtsZ from a medial to a bipolar pattern in *Bacillus subtilis*. *Genes & Development*, **10**, 478–488.
- Lock, R.L. and Harry, E.J. (2008) Cell-division inhibitors: new insights for future antibiotics. *Nature Reviews Drug Discovery*, **7**, 324–338.
- Malanovic, N. and Lohner, K. (2016) Gram-positive bacterial cell envelopes: the impact on the activity of antimicrobial peptides. *Biochimica et Biophysica Acta*, **1858**, 936–946.
- Matsui, T., Yamane, J., Mogi, N., Yamaguchi, H., Takemoto, H., Yao, M., *et al.* (2012) Structural reorganization of the bacterial cell-division protein FtsZ from *Staphylococcus aureus*. *Acta Crystallographica. Section D, Biological Crystallography*, **68**, 1175–1188.
- Monahan, L.G. and Harry, E.J. (2016) You are what you eat: metabolic control of bacterial division. *Trends in Microbiology*, **24**, 181–189.
- Monteiro, J.M., Pereira, A.R., Reichmann, N.T., Saraiva, B.M., Fernandes, P.B., Veiga, H., *et al.* (2018) Peptidoglycan synthesis drives an FtsZ-treadmilling-independent step of cytokinesis. *Nature*, **554**, 528–532.
- Nogales, E., Downing, K.H., Amos, L.A. and Lowe, J. (1998) Tubulin and FtsZ form a distinct family of GTPases. *Natural Structural Biology*, **5**, 451–458.
- Pandey, R., Ter Beek, A., Vischer, N.O., Smelt, J.P., Brul, S. and Manders, E.M. (2013) Live cell imaging of germination and outgrowth of individual *Bacillus subtilis* spores; the effect of heat stress quantitatively analyzed with SporeTracker. *PLoS ONE*, **8**, e58972.
- Paredes-Sabja, D., Setlow, P. and Sarker, M.R. (2011) Germination of spores of *Bacillales* and *Clostridiales* species: mechanisms and proteins involved. *Trends in Microbiology*, **19**, 85–94.

- Paredes-Sabja, D., Shen, A. and Sorg, J.A. (2014) *Clostridium difficile* spore biology: sporulation, germination, and spore structural proteins. *Trends in Microbiology*, **22**, 406–416.
- Piggot, P.J. and Hilbert, D.W. (2004) Sporulation of *Bacillus subtilis*. *Current Opinion in Microbiology*, **7**, 579–586.
- Pinho, M.G. and Errington, J. (2003) Dispersed mode of *Staphylococcus aureus* cell wall synthesis in the absence of the division machinery. *Molecular Microbiology*, **50**, 871–881.
- Ruiz-Avila, L.B., Huecas, S., Artola, M., Vergonos, A., Ramirez-Aportela, E., Cercenado, E., et al. (2013) Synthetic inhibitors of bacterial cell division targeting the GTP-binding site of FtsZ. *ACS Chemical Biology*, **8**, 2072–2083.
- Schaffner-Barbero, C., Martin-Fontecha, M., Chacon, P. and Andreu, J.M. (2012) Targeting the assembly of bacterial cell division protein FtsZ with small molecules. *ACS Chemical Biology*, **7**, 269–277.
- Schuck, P., Perugini, M.A., Gonzales, N.R., Howlett, G.J. and Schubert, D. (2002) Size-distribution analysis of proteins by analytical ultracentrifugation: strategies and application to model systems. *Biophysical Journal*, **82**, 1096–1111.
- Seydlova, G. and Svobodova, J. (2012) Rapid and effective method for the separation of *Bacillus subtilis* vegetative cells and spores. *Folia Microbiologica (Praha)*, **57**, 455–457.
- Steiner, E., Dago, A.E., Young, D.I., Heap, J.T., Minton, N.P., Hoch, J.A., et al. (2011) Multiple orphan histidine kinases interact directly with Spo0A to control the initiation of endospore formation in *Clostridium acetobutylicum*. *Molecular Microbiology*, **80**, 641–654.
- Sterlini, J.M. and Mandelstam, J. (1969) Commitment to sporulation in *Bacillus subtilis* and its relationship to development of actinomycin resistance. *The Biochemical Journal*, **113**, 29–37.
- Stokes, N.R., Baker, N., Bennett, J.M., Berry, J., Collins, I., Czaplowski, L.G., et al. (2013) An improved small-molecule inhibitor of FtsZ with superior in vitro potency, drug-like properties, and in vivo efficacy. *Antimicrobial Agents and Chemotherapy*, **57**, 317–325.
- Sundararajan, K., Vecchiarelli, A., Mizuuchi, K. and Goley, E.D. (2018) Species- and C-terminal linker-dependent variations in the dynamic behavior of FtsZ on membranes in vitro. *Molecular Microbiology*, **110**, 47–63.
- Tan, C.M., Therien, A.G., Lu, J., Lee, S.H., Caron, A., Gill, C.J., et al. (2012) Restoring methicillin-resistant *Staphylococcus aureus* susceptibility to beta-lactam antibiotics. *Science Translational Medicine*, **4**, 126ra135.
- Wagstaff, J.M., Tsim, M., Oliva, M.A., Garcia-Sanchez, A., Kureisaite-Ciziene, D., Andreu, J.M., et al. (2017) A polymerization-associated structural switch in FtsZ that enables treadmilling of model filaments. *MBio*, **8**, e00254–17.
- Wang, H.Y. and Wang, R.F. (2012) Enhancing cancer immunotherapy by intracellular delivery of cell-penetrating peptides and stimulation of pattern-recognition receptor signaling. *Advances in Immunology*, **114**, 151–176.
- Weart, R.B., Lee, A.H., Chien, A.C., Haeusser, D.P., Hill, N.S. and Levin, P.A. (2007) A metabolic sensor governing cell size in bacteria. *Cell*, **130**, 335–347.
- Xiao, J. and Goley, E.D. (2016) Redefining the roles of the FtsZ-ring in bacterial cytokinesis. *Current Opinion in Microbiology*, **34**, 90–96.
- Yang, X., Lyu, Z., Miguel, A., McQuillen, R., Huang, K.C. and Xiao, J. (2017) GTPase activity-coupled treadmilling of the bacterial tubulin FtsZ organizes septal cell wall synthesis. *Science*, **355**, 744–747.

Supporting Information

Additional supporting information may be found online in the Supporting Information section at the end of the article